Ceramics International 48 (2022) 17668–17681

Contents lists available at ScienceDirect

Ceramics International

journal homepage: www.elsevier.com/locate/ceramint

The preparation and characterization of low-temperature foams based on the alkali activation of waste stone wool

Majda Pavlin *, Barbara Horvat, Mark Češnovar, Vilma Ducman

Slovenian National Building and Civil Engineering Institute ZAG Ljubljana, Dimičeva 12, 1000, Ljubljana, Slovenia

ARTICLE INFO

Keywords:
Waste mineral wool
Alkali-activated foams
Porosity
Mechanical properties
Thermal conductivity

ABSTRACT

Waste mineral wool represents a huge amount of construction and demolition waste that is still not adequately returned into the value chain but needs to be landfilled. In the present study, waste stone wool (SW) was evaluated for the preparation of alkali-activated foams. For this purpose SW was milled and sieved below 63 μm, then the activator (sodium silicate) and different amounts of foaming agent (hydrogen peroxide, H_2O_2), varying between 1 wt% and 3 wt%, were added to the slurry and cured in moulds at an elevated temperature (70 °C) for three days. In this way, foamed, highly porous materials were obtained whose density and mechanical properties were influenced by the amount of foaming agent used. The densities obtained ranged between 1.4 and 0.5 g/cm^3, with corresponding mechanical properties of between 12.6 and 1.5 MPa and total porosities in the range 37.8–78.6%, respectively. In the most porous samples with the total porosity of 78.6%, a thermal conductivity of 0.092 W/(m•K) was confirmed. The study confirmed the suitability of waste mineral wool (in our case SW) as a precursor for alkali-activated foams with potential use in the construction sector or other industrial applications.

1. Introduction

Mineral wool is an inorganic material widely used for thermal insulation because of its fire resistance and acoustic comfort. The general term includes glass wool (GW), stone wool (SW), and slag wool, whereby GW and SW are responsible for about 60% of the total wall insulation products on the market [1]. The production of SW accounts for 70% of the total mineral wool production and the estimated value of mineral wool produced in the European Union (data include 28 countries) is about 3 million tonnes in 2020. It has been estimated that Europe generated about 2.55 million tonnes of mineral wool waste in 2020, a large part of which ended up in landfills [2]. In Austria, about 20000–30000 tonnes/year of mineral wool waste was generated, in Slovenia this number is lower due to the population size, but we estimate that it could be in the range of 5000–7500 tonnes/year [3]. Mineral wool wastes are mainly generated by the processes of construction and demolition (C&D), but a small part is also generated during production processes. The composition and cleanliness of the waste differs according to how they were generated, with mineral wool wastes generated during production being easier to recycle as the composition of the waste is known [4]. C&D wool waste can consume a lot of space in landfill because the density of mineral wool (waste) is low. It is therefore crucial to reduce this waste by using it as a raw material in new products, such as foamed products. The majority of foamed products are produced at an elevated temperature. Melting is a commonly used method for the preparation of lightweight foamed glass. Mineral wool has been thermally treated in addition to waste glass for the synthesis of foam glass using calcium carbonate, borax, and sodium phosphate as additives to act as the fluxing agent and foam stabiliser. The mixture of 40 wt% mineral wool waste, 60 wt% waste glass, 20 wt% borax, 1–2 wt% calcium carbonate, and 2 wt% sodium phosphate was thermally treated at 800 °C. At this optimum condition, the mixture exhibited a uniform foam structure and a low bulk density of 0.7 g/cm^3 [5]. In a study by Chen et al., ceramic foams were prepared through high-temperature treatment of waste mineral wool and waste glass, using SiC as a foaming agent. A mixture of 40 wt% mineral wool, 50 wt% waste glass, 10 wt % silica sand, and 2 wt% SiC was proposed as the optimum ceramic foam, which was thermally treated at 1170 °C with a heating rate of 20 °C/min and a holding time of 20 min at the selected temperature. The ceramic foams produced had a bulk density of 0.71 g/cm^3 and a uniform pore size distribution. However, with the higher percentage of mineral wool (from 30 to 40 wt%), the thermal treatment at 1170 °C decreased the pore size (from 0.5-1.5 mm to 0.3-0.5 mm) due to the lower number of alkali cations (Na^+, K^+, Mg^{2+}, and Ca^{2+}), which increased the

* Corresponding author. Slovenian National Building and Civil Engineering Institute, Dimičeva 12, 1000, Ljubljana, Slovenia.
E-mail address: majda.pavlin@zag.si (M. Pavlin).

https://doi.org/10.1016/j.ceramint.2022.03.037
Received 20 December 2021; Received in revised form 28 February 2022; Accepted 3 March 2022
Available online 11 March 2022

viscosity of the liquid phase [6]. The main advantage of the alkali-activated foams (AAFs) over the production of sintered vitreous foams is significantly lower energy consumption since AAF can be produced at the temperatures lower that 100 °C while for the productions of foamed glass or sintered foams temperature about 800 °C or higher should be utilized [7,8]. Reported density of foamed glass can go down to the 0.15 g/cm^3 [8] while reported density of AAF are down to the 0.3 g/cm^3 [9]. Depending on the precursors (e.g. slag, metakaolin) AAF can be stable even up to 900 °C [10] what is not the case with foamed glass neither with AAF based on mineral wool due to the glass softening at lower temperatures. Not many studies, however, mention alkali activation as an approach to produce lightweight mineral wool samples. To date there are some studies that address this, however, all of them used GW or SW as a co-binder with other precursor(s) in the alkali-activated mixture and not solely GW and SW. In the study of Erofeev et al. mineral wool production waste was used to prepare alkali-activated lightweight material, using NaOH as the alkaline activator, aluminium powder as a foaming agent, larger particles of mineral wool waste as a fine aggregate, and a water-holding additive. Average densities for various lightweight AAFs ranged from 0.61 to 1.13 g/cm^3, compressive strength from 1.7 to 5.4 MPa, and thermal conductivity from 0.144 to 0.345 W/(m•K) [11]. The second study, carried out by Alzaza et al. developed a fibre-reinforced alkali-activated lightweight mineral wool-based mortar using various premade foam and polypropylene fibres to improve the mechanical properties of the alkali-activated material (AAM). To promote a durable final product, metakaolin was included in all compositions. The lightweight blends varied in the proportion of SW and GW (weight ratios SW50:GW10 and SW30:GW30), while the content of metakolin was constant at 40 wt%. Densities ranged from 0.77 to 1.51 g/cm^3, compressive strengths from 1 to 9 MPa and bending strengths from 2.6 to 8 MPa. A higher SW/GW ratio in the fibre-reinforced AAF showed better workability but lower density of mixtures. However, higher density in SW50/GW10 compared to SW30/GW30 increased the rate of strength [12]. In the study of Kozub et al. 3 or 5 wt% of waste glass wool was added to the alkali-activated foamed fly ash (FA) composites. Improvement in compressive strengths and reduction in the density and heat conduction coefficient were observed. The reference sample without the addition of GW showed a compressive strength of 2.8 MPa, while an improvement was observed for 10% with 3 wt% and for 20% (3.4 MPa) with the addition of 5 wt% GW. The thermal conductivity coefficient with 5 wt% GW added decreased from 0.121 to 0.113 W/(m·K) compared to the reference sample without GW addition whereas the density dropped from 0.62 to 0.5 g/cm^3 [13].

In the alkali activation of foamed/lightweight materials, several known and new methods are proposed to produce this type of porous material, all of which use a low low-temperature process compared to thermal treatment or glass foaming. One possibility is to use prefabricated lightweight granules mixed with alkali-activated ground granulated blast-furnace slag (GGBFS) binder [14]. Another option is to foam the binder itself, for which mechanical, thermal or chemical foaming methods are used. Mechanical foaming, or the direct introduction of air into the mixture, is done using a high-speed mixer. Thermal foaming is useful when the precursor's composition allows the material to expand at a higher temperature. Erdoğan studied heat-treated perlite activated with NaOH, but there were some disadvantages, such as a decrease in pH during heat treatment, resulting in a lower porosity [15]. With the heat treatment process controlling porosity can be very difficult, due to changes in the viscosity and texture of the material. Chemical foaming is mainly used to process foam with a predictable pore volume and size distribution, which can be achieved by controlling the amount of foaming agent added. Hydrogen peroxide (H_2O_2) is a well-accepted gas releasing agent and one of the agents commonly used to foam AAM [12,16–24]. The chemical reaction can also produce gases in highly basic media when metals such as Al, Si, or Zn are incorporated and cause an expansion of the material [25]. Knowing the reactivity rate, the porosity can be formulated, but in the case of foaming, physical effects also grow in the expansion region, making it critical for air bubbles to collapse or for smaller ones to reform into larger ones. For this reason, the resulting density, or corresponding heat/noise insulation, can not be achieved. Various surfactants, also called stabilisers, are used, and through their addition, the porosity can be controlled by reducing the surface tension of the air bubbles. Stabilising agents are added to the mixture to provide stable air bubbles from foaming throughout the expansion and while curing. Anionic surfactants such as sodium dodecyl sulfate (SDS), which are commercially available for other purposes, are commonly used as a stabilising agent in the fabrication of porous structures through alkali activation. The effect of SDS on the development of porosity was studied by Korat and Ducman, where material foamed with H_2O_2 was stabilised using seven differing amounts of SDS. The authors concluded that the stabilising agent needs to be adjusted in proportion to the quantity of the foaming agent [17]. Natural substances such as vegetable oil can also be used for stabilization, as confirmed by Bai et al., where different types of oil were evaluated and found to be suitable for use in foaming [26].

In this study, waste SW was used to prepare AAFs using H_2O_2 as a foaming agent and Triton as a pore stabiliser. This is the first study where waste SW has been used as a sole precursor for the preparation of lightweight AAFs. Milled mineral wool is composed of fibres and serves simultaneously as a binder (smaller particles that dissolved during alkali activation) and as fibres to reinforce the foams (not all mineral wool dissolves in alkali, as demonstrated in our previous [27] and other studies [28,29]), and therefore no additional fibres were added to the mixture. The use of powdered SW as a precursor in alkali activation increases the bending strength simply because of the elongated shape of the parts, which do not react completely. However, smaller particles (fibres) are needed for a higher rate of alkali activation. Our previous studies have shown that smaller particles of FA and particles of refractory materials improve the mechanical properties due to the larger surface area and thus the larger surface area available for alkali activation [30,31]. Mineral wool fibres below 63 μm were found to have much better workability than the particles, e.g. below < 125 μm. Due to the variable particle size of the mineral wool, the workability of the blends varies, so that in the case of larger particles, more sodium silicate was required [32]. In the present study different proportions of H_2O_2 and Triton were used in the preliminary research to determine the optimal proportions for the mix design. The addition of 1.5 wt% Triton with either 2.5 wt% or 3 wt% of H_2O_2 was found to be the optimal choice; the addition of different amounts of H_2O_2 was also investigated in order to evaluate the effect of added a foaming agent on the microstructure of the foamed alkali-activated mineral wool. The detailed study includes mechanical properties, X-ray diffraction (XRD), Fourier transform infrared spectroscopy (FTIR), microstructural properties (scanning electron microscopy – SEM micrographs and figures obtained using an optical microscope), the porosity of the foams (measured by mercury intrusion porosimetry – MIP), and thermal conductivity to evaluate the differences in the production of the foamed material.

2. Materials and methods

2.1. Materials and sample preparation

SW needs to be milled to get fine powder material with the properties of the binder. SW (the composition of which is given in Table 1) was milled in a concrete mixer (Altrad CE-350, United Kingdom) for 4 h and then for an additional 2 h in a ceramic dish (Elektrokovina, Slovenia) using steel balls. Following milling, all material was sieved to below 63 μm and homogenised for further use (for sieving Retsch AS200 Control-g Vibratory Sieve Shaker, Germany, was used). The particle size distribution of the milled SW is presented in Fig. 1 (measured by Microtrack Sync, USA, Pennsylvania). The presence of bigger particles results from longer fibres entering perpendicularly through the sieve (Retsch, Germany).

Table 1
Chemical composition of the major oxides present in the SW (wt%), LOI at 950 °C, BET specific surface area and humidity of the SW used for the preparation of AAF.

	SiO_2 (wt%)	Al_2O_3 (wt%)	CaO (wt%)	Fe_2O_3 (wt%)	MgO (wt%)	Na_2O (wt%)	Other oxides (wt%)	LOI (wt%)	BET (m^2/g)
SW	38.4	17.2	16.1	6.45	12.0	2.00	3.25	4.60	0.4852

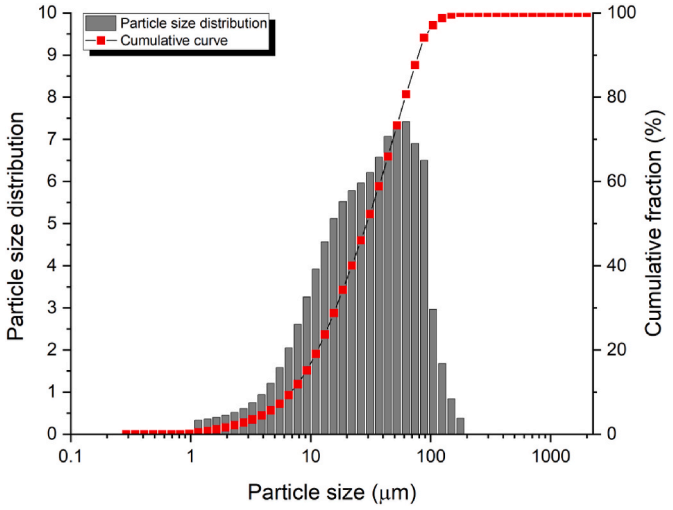

Fig. 1. Particle size distribution of the milled waste stone wool (SW).

The data of chemical composition analysis obtained by X-ray fluorescence (XRF), loss on ignition (LOI) and Brunauer–Emmett–Teller (BET) analyses of the waste mineral wool are presented in Table 1.

Lightweight AAM were prepared using 75 g SW sieved to below 63 μm, 54 g sodium silicate (Geosil 34417, produced by Woellner, SiO_2: Na_2O = 1.68, 55.6 wt% H_2O), and 15 g distilled water. The selection of the amount of ingredients in the selected mixtures using SW, sodium silicate and additional water was based on experience from previous work with alkali-activated SW [27] and additional experiments conducted for the purposes of this work. The results of the mechanical properties are shown in Table 2. Since the mixture should be workable but not too liquid to ensure good AAF performance, water was added to the mixture. Not all mixtures showed good workability, and the one with good workability and the best mechanical properties was selected (see bolded mixture design in Table 2).

Table 2
The preliminary experiments for various mix designs with the data for compressive and bending strengths. Designations for each mix design represents the type of used ingredient such as SW, NaSi (sodium silicate) and H_2O (water) and in the brackets there are the masses of used ingredients (in grams).

Mix design	Compressive strength (MPa)	Bending strength (MPa)	Mixing and moulding of the mixture
SW(75)NaSi (65)	16.8 ± 0.31	7.28 ± 0.51	Possible
SW(75)NaSi (60)	18.3 ± 1.16	6.25 ± 0.87	Hard mixing and moulding
SW(75)NaSi (55)	27.7 ± 2.70	7.51 ± 0.07	Hard mixing and moulding
SW(75)NaSi (45)	44.4 ± 2.05	15.3 ± 0.41	Hard mixing and moulding (almost impossible)
SW(75)NaSi (54)H_2O (15)	**19.6 ± 3.25**	**4.00 ± 0.29**	**Possible**
SW(75)NaSi (50)H_2O (10)	17.5 ± 1.05	5.15 ± 0.18	Possible but less workable as with SW(75)NaSi(54) H2O(15)
SW(75)NaSi (38)H_2O (10)	29.7 ± 0.49	4.64 ± 0.15	Hard mixing and moulding
SW(75)NaSi (38)H_2O (20)	12.2 ± 1.45	3.47 ± 0.06	Possible

In all mix designs, the water to binder ratio (W/B, SW acts as a binder) was 0.60 (the water contained in the sodium silicate and additional water added were taken into account in the calculation and divided by mass of SW). Varying amounts (1–3 wt%) of a hydrogen peroxide solution (30% liquid, H_2O_2, Carlo Erba reagents, Barcelona, Spain) was added as a foaming agent, and a non-ionic surfactant, Triton X-100 (Dow Chemical Company), was added as the stabilising agent. A detailed description of the sample compositions is presented in Table 3. Liquid chemicals were chosen as foaming agents and stabilisers because the reactive components distribute more evenly than when dry foaming agents and stabilisers are used in the reaction. The sample mixtures were gently mixed manually then placed in moulds with nominal dimensions of 20 × 20 × 80 mm^3. The moulds were then placed in an oven at a temperature of 70 °C for three days to reach the final compressive and bending strengths. The resulting hardened test specimens were then demoulded and stored at a controlled temperature of 20 ± 2 °C.

2.2. Characterization of the samples

The mineral composition of the SW waste and alkali-activated SW was evaluated using an XRD (Malvern PANalytical Empyrean, Surrey, United Kingdom) with a CuKα radiation of λ = 0.154 nm. The intensity was scanned in the 2θ range from 4° to 70°, in steps of 0.026°/min. The data was analysed with X'Pert High Score Plus diffraction software from PANalytical (Malvern PANalytical Empyrean, Surrey, United Kingdom), using database PDF 4 + 2015 RDB powder diffraction files from the Inorganic Structure Database (ICSD).

XRD of alumina oxide powder as an external standard reference material (NIST 676a) was performed for quantitative analysis control of the multiphase mixtures using Rietveld refinement of the powder XRD. Rietveld refinement was performed using X'Pert High Score Plus diffraction software, with the goodness of fit determined for each measurement.

The specific surface area (BET) of the milled and sieved SW (below 63 μm in size) was determined by nitrogen adsorption at 77 K over a relative pressure range of 0.05–0.3 (Micromeritics ASAP 2020, Micromeritics, Norcross, GA, USA). Before the BET analysis, samples were exposed to a temperature of 70 °C for 24 h and degassed to 0.133 Pa (Micromeritics Flowprep equipment, Micromeritics, Norcross, GA, USA).

After 3 days of curing at 70 °C and after 28 days cured at room temperature the bending and compressive strengths of the alkali-activated SW foams were measured using a Toninorm instrument (ToniNORM, ToniTechnik, Berlin, Germany) at a constant force rate of 0.05 kN/s. Bending and compressive strengths were measured on 4

Table 3
The sample designations and compositions of the different mixtures prepared.

Sample	SW (g)	Sodium silicate (g)	H_2O (g)	H_2O_2 (wt %)[a]	Triton X-100 (wt %)[a]
F1	75	54	15	1	1.5
F2	75	54	15	1.5	1.5
F3	75	54	15	2	1.5
F4	75	54	15	2.5	1.5
F5	75	54	15	3	1.5

[a] Mass calculated on mass of stone wool (SW).

prisms (20 × 20 × 80 mm^3). After measuring bending strengths, remaining prisms' halfs were used for compressive strengths.

The macrostructure of the AAM samples was investigated by optical microscope (Nikon, SMZ18), while the microstructure was assessed using a SEM (JSM-IT500LV, Jeol, Tokyo, Japan) equipped with an energy dispersive X-ray analyser (EDXS, Link Pentafet, Oxford Instruments). Back-scattered electron (BSE) detection was applied using polished foamed samples prepared in epoxy resin and observed under low vacuum conditions.

For thermal conductivity measurements, samples were prepared in 100 × 100 × 30 mm^3 moulds. The thermal conductivity was measured in an air atmosphere using a heat-flow meter (HFM; HFM 446 Lambda Small, Stirolab, Sežana, Slovenia) following the EN 12667, ASTM C518 and ISO 8301 standards. The area of the heat-flow meter was 40 mm × 40 mm^2. The instrument was calibrated by measuring a NIST Standard Reference Material® 1450d. The typical accuracy of the HFM is ±1%. The measurements were performed at a 10 °C middle sample temperature and a 13 °C temperature difference.

To obtain an infrared spectrum of the alkali-activated SW products FTIR (Perkin Elmer Spectrum two, Kentucky, USA) equipped with an attenuated total reflection accessory (Universal ATR) was applied, using a diamond/ZnSe crystal as a solid sample support in the range from 400 to 4000 cm^{-1} at a resolution of 4 cm^{-1}.

Following the processes of curing and drying, MIP was performed on the AAM samples using a mercury porosimeter (Micromeritics, Norcross, GA, USA). Samples were dried for 24 h before measurement and then analysed using Micromeritics®Autopore IV 9500 equipment (Micromeritics, Norcross, GA, USA). MIP experiments were conducted on samples that had been cured at room temperature up to 28 days. The true density of solid powdered samples was measured with an UltraPyc 1200e (Anton Paar) using an inert gas to measure the sample volume by applying Archimedes' principle of displacement.

3. Results and discussion

3.1. Preliminary studies

The preliminary work was performed using H_2O_2 as a foaming agent and Triton as a pore stabilising agent in order to access the influence of their proportions on the mechanical properties (bending and compressive strengths) and density of the AAFs (Fig. 2). The W/B ratio and curing temperature were the same in all experiments. Curing at 70 °C for 3 days was selected for all experiments, firstly to prevent the collapse of bubbles in the paste, since the stability of the foam depends on the reaction kinetics and hardening time [33], and, secondly, because in alkali-activated waste SW early strength is achieved later compared to in other precursors suitable for alkali activation [34]. In previous work where ladle and electric arc furnace slags were alkali-activated, almost identical (bending/compressive) strength was obtained with a 3-day cure at 70 °C as with a 28-day cure at room temperature [35]. The same conditions were applied to AAFs based on FA, where different foaming agents and stabilisers were investigated [36]. Three days at 40 °C for alkali-activated mineral wool specimens had similar mechanical properties to 28 days of room temperature curing, but did not reach the final strength (which increased even after 90 days of room temperature curing), as demonstrated in our previous study [27]. Therefore, a three-day cure at 70 °C was selected for the production of AAFs from waste SW assuming that we achieve final strength. The density and mechanical properties measured in these foams are presented in Fig. 2. The densities measured decrease in line with the increasing percentages of foaming and stabilising agents. When 1 wt% H_2O_2 was used, optimal porosity could not develop, and the densities measured were therefore the highest (over 1.3 g/cm^3). By using 1.5 wt% of H_2O_2, the measured density dropped below 1.3 g/cm^3 when at least 1.5 wt% of Triton was used. No additional decrease in density was observed, however, when the amount of Triton added ranged between 1.5 and 2.5 wt%. A significant decrease in density was measured following the addition of both 2 wt% (0.86–0.88 g/cm^3) and 2.5 wt% H_2O_2 (0.69–0.79 g/cm^3). The lowest densities, with values between 0.63 and 0.65 g/cm^3, were achieved in the foams where 3 wt% H_2O_2 was used. The mechanical properties of foamed samples correlated with their densities. Compressive strengths were highest when 1 wt% H_2O_2 was used. A drop in compressive strength was observed at elevated proportions of H_2O_2, especially with the addition of 2% H_2O_2. The amount of stabilising agent affects the mechanical properties when 1 or 1.5 wt% H_2O_2 was added, but not at higher proportions of H_2O_2. Compressive strengths were in the range 2.0–2.7 MPa when 3 wt% H_2O_2 was used. The values of bending strength were between 1.5 and 4.0 MPa, with the lowest values, between 1.5 and 1.8 MPa, being measured in the foamed samples prepared using 3 wt% H_2O_2. In general, increasing the amount of foaming or stabilising agent had a greater effect on the compressive strength, as can be seen from the variable results (1.7–22.5 MPa), resulting in more porous samples. Such an impact was not observed so strongly in relation to the bending strength, which only varied between 1.5 and 4 MPa across all the samples prepared. The improvement in bending strength when using waste mineral wool is due to the many unreacted particle-fibres in the alkali-activated matrix [27].

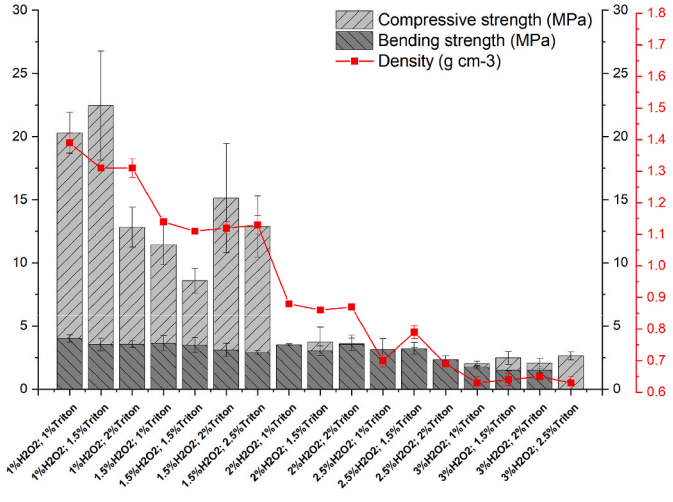

Fig. 2. Density, bending and compressive strength of the alkali-activated mineral wool foams (and their standard deviations) made using H_2O_2 as the foaming agent and Triton as the stabilising agent.

3.2. Mechanical properties of selected AAFs

To evaluate the effect of different mass percentages of H_2O_2 on the microstructure and porosity of lightweight AAMs, we prepared samples with 1.5 wt% of Triton and 1, 1.5, 2, 2.5 and 3 wt% H_2O_2. Although a higher amount of surfactant may lead to a higher porosity, we fixed this parameter and evaluate the influence of the foaming agent, as done in the study by Masi et al. [22]. All five samples were cured at 70 °C for 3 days and then at room temperature until 28 days. In order to check the stability of the prepared samples, mechanical properties were measured after 3 and 28 days (Fig. 3). After 3 days, the density dropped in all samples with the increasing amount of H_2O_2. A slight increase in density was seen in all samples following curing at room temperature until 28 days. Significant changes were observed in the samples with 1–2 wt% H_2O_2 added, with densities rising from 1.26 to 1.45, 1.03 to 1.26 and 0.82–0.90 g/cm^3 in samples F1, F2 and F3, respectively. Increased densities were also observed in the F4 and F5 samples, from 0.62 to 0.67 g/cm^3 in the F4 sample and 0.50–0.54 g/cm^3 in the F5 sample.

As expected, after 3 days of curing at 70 °C the strength values began to decline when the foaming agent was increased from 1 to 3 wt%, with compressive strength dropping from approximately 11.9 to 1.64 MPa,

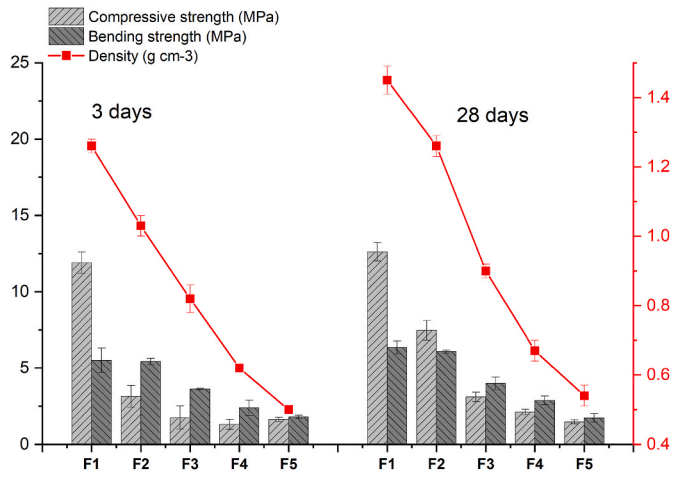

Fig. 3. The results of densities, bending and compressive strength of the measured alkali-activated mineral wool foams made by using 1–3 wt% H_2O_2 and 1.5 wt% of Triton with the standard deviations. Samples were cured for 3 days at 70 °C and then at room temperature up to 28 days.

and bending strength from 5.51 to 1.79 MPa. A similar trend was observed in all samples after 28 days, with compressive strength falling from 12.6 to 1.47 MPa, and bending strength from 6.35 to 1.73 MPa. Following curing for 3 days at 70 °C, and then at room temperature until 28 days, values of compressive strength showed a slight increase in sample F1, whereas it almost doubled in F3, and more than doubled its initial value in the F2 sample. After 28 days the compressive strength had increased in F4 but decreased in F5. An increase in compressive strength after 28 days was also observed in another study, where circulating fluidised bed fly ash was used to prepare AAFs, with H_2O_2 used as the foaming agent [23]. Bending strength slightly increased in the F1–F4 samples after 28 days of curing, while in the F5 sample the values remained similar to those following 3 days curing at 70 °C. The experiments show the influence of foaming agents on the mechanical properties of foams, where lower densities were achieved in samples with an elevated proportion of H_2O_2, particularly in samples F4 and F5. It should be noted that the curing process is not fully complete after 3 days at 70 °C, as indicated by the improved mechanical strengths after 28 days (Fig. 2). Measurement errors should, however, be taken into account at lower values of compressive and bending strength.

3.3. Macro and microstructures of AAFs

Fig. 4 and Fig. 5 show images of the foamed samples with 1.5 wt% Triton and different mass proportions of H_2O_2 (between 1 and 3 wt%). Fig. 4 shows the macrostructures of samples F1–F5, while the microstructures of the foams are presented in Fig. 5. Fig. 4 clearly shows the influence of elevated amounts of H_2O_2, causing an increase in the macroporosity of the structure. It can be seen that pores are both spherical and non-spherical in shape, and they are non-uniformly distributed. It can be seen in Fig. 5 that samples F1 and F2, with H_2O_2 concentrations of 1 and 1.5 wt% respectively, share a similar microstructure; the addition of 1.5 wt% of H_2O_2, however, results in the presence of bigger pores. In both cases, the larger pores are spherical, but many micro-cracks are also observed in the matrix. With the addition of 2 wt% H_2O_2 to the mixture, a significantly higher porosity was observed, along with the presence of randomly distributed spherical and non-spherical pores. The addition of 2.5 wt% H_2O_2 resulted in many irregular interconnected pores compared to when 2 wt% H_2O_2 was used. The pores were much bigger compared to when 1–2 wt% H_2O_2 was added. At 3 wt% H_2O_2 the interconnection into bigger pores (coalescence) was more significant. Non-spherical interconnected pores reached a pore size larger than 2 mm. Micro-cracks are present in all samples, but fewer micro-cracks are observed in the matrices of the samples with 2.5 and 3 wt% H_2O_2 (Fig. 5). A more compact matrix may form in this sample due to the easier evaporation of water and/or elevated gas pressure resulting from the decomposition of H_2O_2. The matrix is evident in all samples as a result of alkali activation. Many unreacted fibres could, however, also be seen. Although the higher proportion of H_2O_2 increased expansion, causing a higher porosity and thus bigger pores, the interpore connections (matrix) are similar in all cases. The irregular shape of pores with a large size distribution can lead to the formation of a complex network of interlinking air channels.

SEM-EDXS point analysis was performed to calculate the Si/Na, Si/Al, Na/Al and Ca/Si ratios in the AAFs (presented in Table 3). The elemental ratios in the AAMs were also calculated using XRF (Table 1) and XRD measurements of SW precursor before alkali activation and addition of sodium silicate (calculations were performed using the study by Horvat et al. [37]). The data show lower values for Si/Na, Si/Al and Na/Al ratios, while the Ca/Si value is higher. The Si/Al ratio influences the compressive strength of AAMs, and all foams show a ratio between 5.30 (F1) and 5.83 (F4). Considering that almost 100% of material is in the amorphous phase, a higher Si/Al ratio compared to XRF data indicates a better dissolution of silicon compared to aluminium. This statement is also proven by the higher Si/Na and Na/Al ratios. The F1 sample, which has the highest compressive strength, did not have the highest Si/Al ratio. The optimal Si/Al ratio stated for alkali-activated metakaolin has varied amongst the literature, from 1.9 [38], to 3.3 [39] and 4 [40]. In the study by Hajimohammadi et al. it was found that in GGBFS an elevated Si/Al ratio (from 3.6 to 4.5) caused wider pore size distribution. The higher Si/Al ratio in samples F4 and F5 suggest better polymerization compared to samples F1–F3, which may be attributed to the formation of small and closed pores that hinder the removal of water when cured [41]. Incomplete dissolution was observed in the F1–F5 foams due to the presence of undissolved fibres, as can be seen in Fig. 5. The Si/Na ratio was higher compared to data calculated from XRF, however, confirming the dissolution of silicon. Due to the high Na/Al ratio in all the foamed samples (greater than 1.65), while the recommended values are around 1 or less [42], the efflorescence was expected, as confirmed by the XRD experiments in Fig. 6 (see below in subchapter

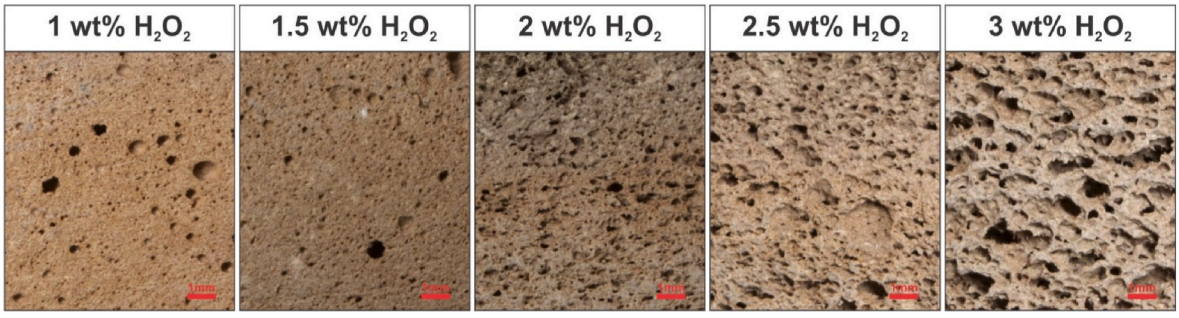

Fig. 4. Macrostructure of five samples with 1–3 wt% H_2O_2 used as the foaming agent and 1.5 wt% of Triton as the stabilising agent.

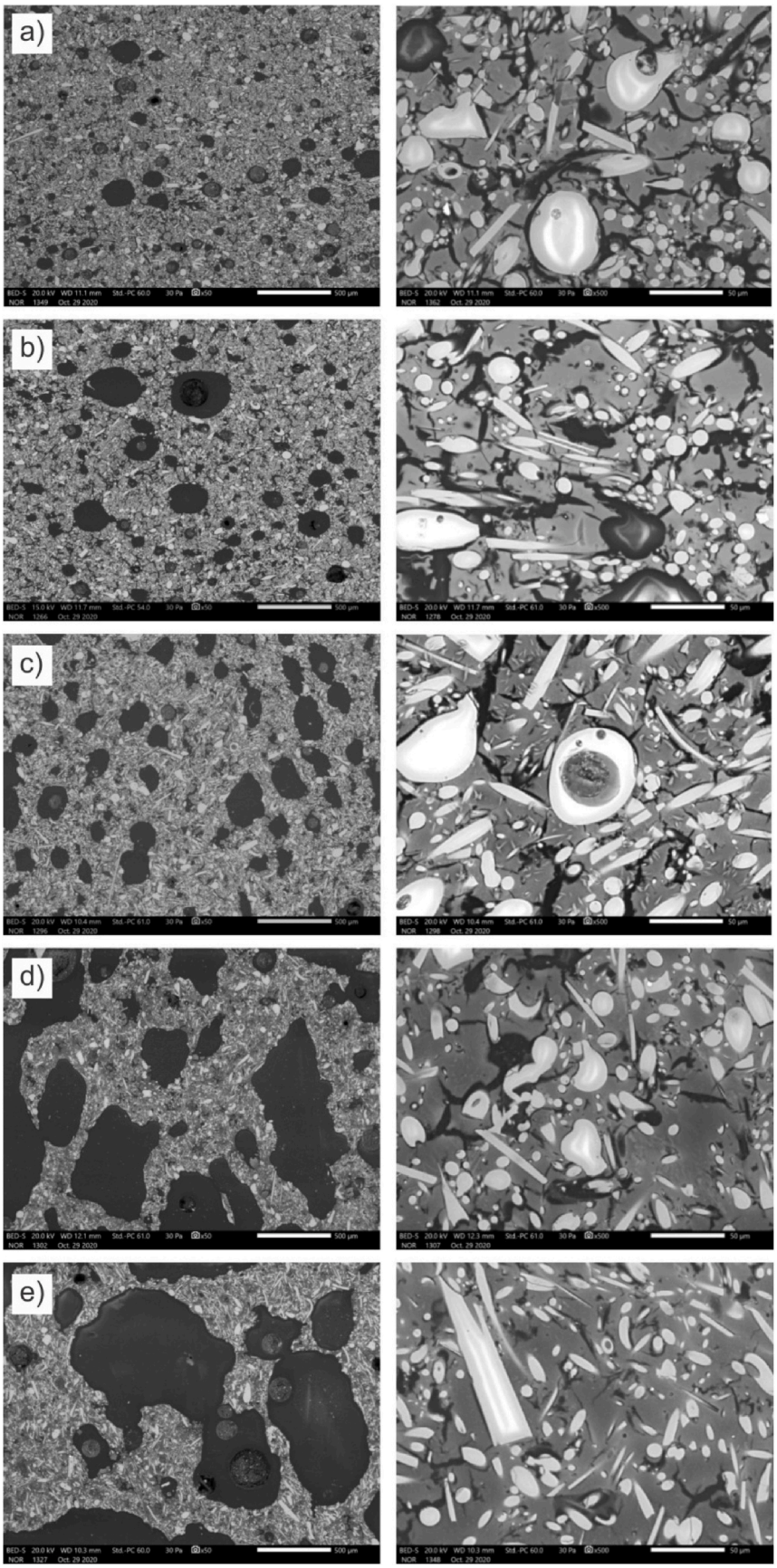

Fig. 5. SEM micrographs of the five samples with a) 1 wt%, b) 1.5 wt%, c) 2 wt%, d) 2.5 wt% and e) 3 wt% of H_2O_2 used as the foaming agent and 1.5 wt% of Triton as the stabilising agent. SEM microstructures are 50-times magnified on the left and 500-times on the right.

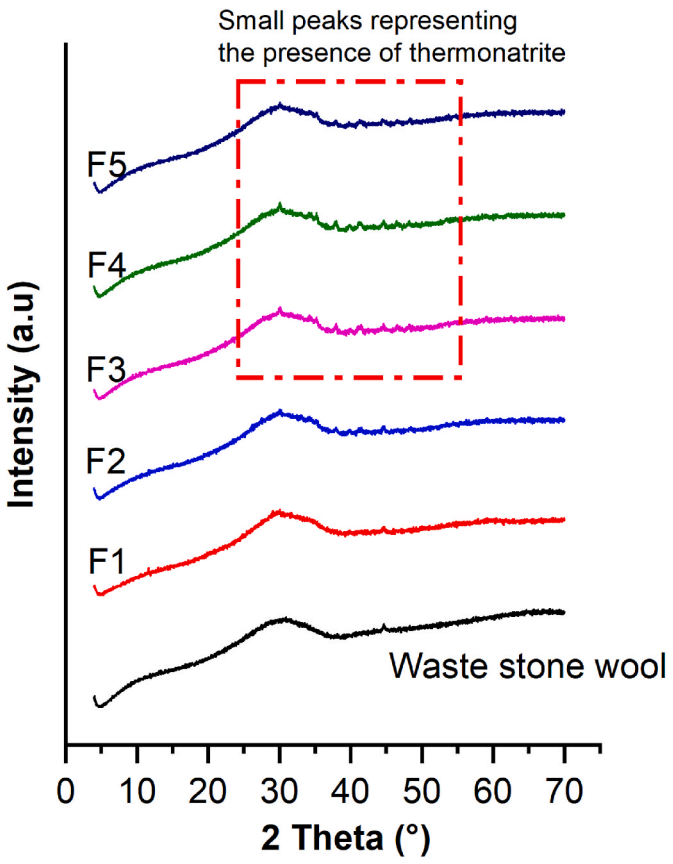

Fig. 6. Diffractograms of waste SW and alkali-activated foams F1–F5 using 1.5 wt% stabilising agent and 1–3 wt% foaming agent.

3.4. *Mineralogical information*). Curing at temperatures ≥ 65 °C may significantly affect efflorescence reduction, leading to higher total porosity and larger pore size [25]. Although AAFs were exposed to 70 °C, crystallites of thermonatrite were observed after 28 days (Fig. 6). Dissolution of calcium is favoured in all foam samples since sodium silicate was used, rather than NaOH, which (due to the high pH) hinders its dissolution [43,44]. The Ca/Si ratios decrease from F1 to F5, however, as a result of the dissolution of silicon.

3.4. Mineralogical information

XRD analysis was performed to determine the presence of amorphous phase in each foamed sample and to identify differences in the mineralogical structures after 28 days (Fig. 6). More than 99% of the material is in the amorphous phase both before (presented as waste SW) and after alkali activation. It was not therefore possible to define Rietveld refinement in the F1 and F2 samples. The F3–F5 samples show a few small peaks, however, representing the presence of thermonatrite (less than 0.7%, obtained by Rietveld refinement) due to efflorescence on the surface. The presence of thermonatrite is expected due to the insufficient solubility of Si and Al from SW (many unreacted particles are seen in the SEM pictures in Fig. 5) and the consequent presence of excess sodium. The goodness of fit in samples F3–F5 was between 5.56 and 5.59, which is greater than the ideal value (an ideal value is 1), and is a consequence of the deconvolution of a very small peak which ends with a bigger error. The halo, typical of an amorphous phase, shifted slightly towards higher 2θ values following alkali activation.

Our previous study showed more unreacted particles of SW compared to GW after alkali activation with sodium silicate, but in both cases unreacted wool fibres are present [27]. In another study, it was confirmed that more GW dissolves in NaOH than SW [45]. If all SW fibres dissolved, there would be only a small excess of sodium, as can be seen from the Na/Al ratio, which indicates the value of 1.17 (Table 4, first column, where the data obtained from XRF were included in the calculation considering 100% amorphous phase for SW). But due to the incomplete dissolution, the Na/Al ratio in F1–F5 is higher than 1.17. Since the porosity in samples F3–F5 is much higher than in F1 and F2 despite the comparable or even lower Na/Al ratio (e.g., in sample F5), the easier diffusion of sodium due to the larger pores and the larger surface area available for the reaction between moisture and CO_2 favours the formation of thermonatrite. As Zhang et al. stated, efflorescence is the phenomenon in which the internal alkalis are carried to the surface and provide Na^+ for precipitation of sodium carbonates until an equilibrium state (saturation) is reached between the pore solution and the crystals [46]. The phenomenon of subflorescence, on the other hand, occurs when crystallisation occurs at depth in the pores of the solid matrix, allowing the uptake of dissolved CO_2 [47]. Rapid efflorescence is related to higher porosity [48], which is consistent with the results in Fig. 6, where the more porous samples F3–F5 show thermonatrite, while this cannot be confirmed for the less porous samples F1 and F2. According to the study by Yliniemi et al., in SW, activated with sodium silicate, a C-(N-)A-S-H type gel with low Ca content and maximum incorporation of Al and Na forms as the main binding phase, while the excess alkali and freely available Si and Al drive the formation of an additional Al-rich N-A-S-H gel reaction product [28]. Although it is believed that in a low Ca system, more Al is dissolved and higher Al content leads to higher Na^+ incorporation [49], in the SW alkali-activated system, many fibres did not dissolve during the alkali activation process, leaving Na^+ in excess, leading to the efflorescence. Similar results on efflorescence were found in the study by Alzaza et al. where they found that more efflorescence can be expected in the case of SW, with a higher SW content in mixtures of SW and GW having a greater effect on increasing efflorescence [12].

3.5. FTIR analysis

Fig. 7 shows FTIR results of the lightweight AAFs after preparation (t = 0), following curing at 70 °C for 3 days, and then after curing at room temperature until 28 days. The spectra for sodium silicate and waste SW are also shown. The position of the Si-O-T (T = Al, Si) asymmetric stretching band for the SW precursor is located at 891 cm^{-1}. The sodium silicate solution shows three overlapping bands, located at about 1100, 986 and 890 cm^{-1}, which are assigned to the respective vibrations of silicate polymers, smaller molecules (monomer to tetramer), and small anionic species [50,51]. The dissolution and polymerization of the mixture could be observed at the beginning (FTIR spectra at t = 0), with the absorbance band attributed to the stretching of O-H seen at around 3338–3353 cm^{-1}, and the bending of the O-H bond at about 1640–1650 cm^{-1}. These two peaks disappeared after curing at 70 °C for 3 days, due to the removal of water. The bands between 980 and 990 cm^{-1} can be primarily attributed to the stretching of the Si-O-Si bond from sodium silicate, and are modified and shifted to lower values (compared to sodium silicate) due to the alkali activation of the mixture with the polycondensation reaction and rearrangements of the Si-O-T bonds. On the other hand, the shoulder of the band at about 872 cm^{-1} is attributed to the asymmetric stretching vibration band of Si-O-T (T = Al, Si),

Table 4
Si/Na, Si/Al, Na/Al and Ca/Si ratios in samples F1–F5, as obtained by point analyses on aluminosilicate matrix (SEM-EDXS), and the data of precursor calculated from XRF.

	XRF data	F1	F2	F3	F4	F5
Si/Na	2.14	2.80	2.37	2.39	3.23	3.34
Si/Al	2.52	5.30	5.35	5.34	5.83	5.50
Na/Al	1.17	1.89	2.26	2.59	1.80	1.65
Ca/Si	0.30	0.25	0.25	0.21	0.20	0.20

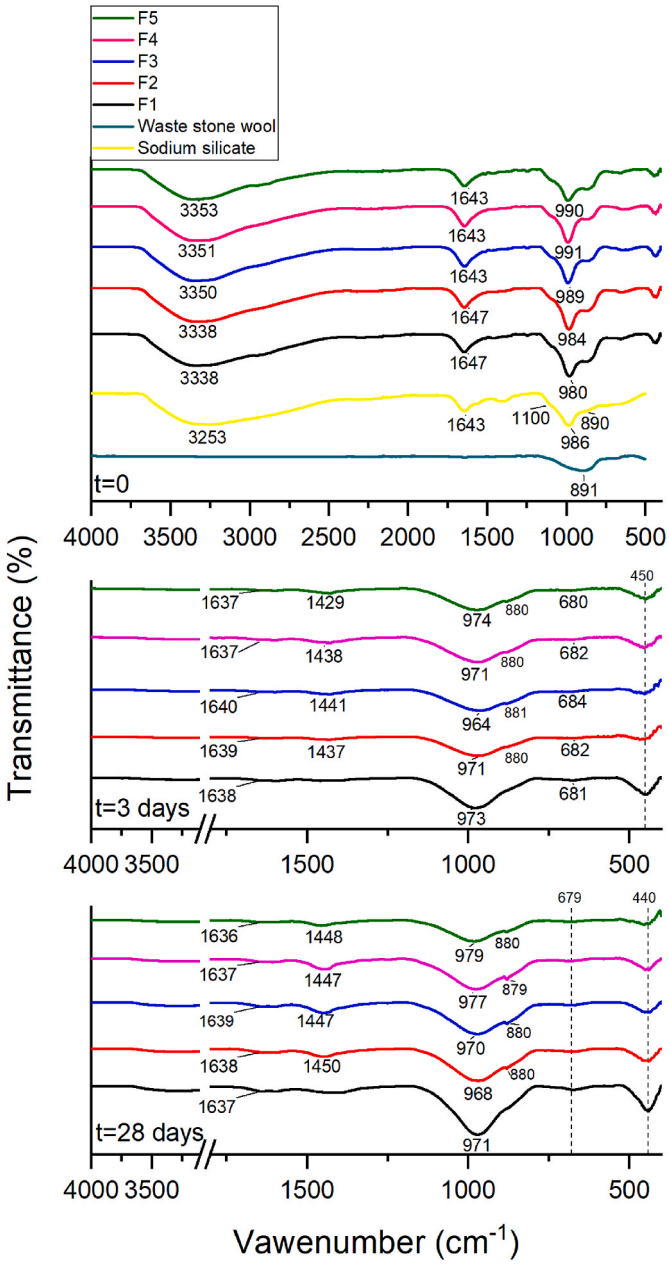

Fig. 7. FTIR spectra of the alkali-activated wool waste mixtures F1–F5 after preparation (t = 0), following 3 days curing at 70 °C, and after curing at room temperature until 28 days.

explained by the dissolution of the powdered SW. The main band changes over time and becomes smoother, with no shoulder present in the spectra after 3 days curing at 70 °C, at which point most of the alkali activation has been completed.

After 3 days curing at 70 °C, the main Si-O-T asymmetric stretching band shifted to higher values, of between 964 and 974 cm^{-1}, when the alkali activation process is introduced. This shift, from about 872 cm^{-1} to higher values, occurs due to the rearrangement of the Si-O-T (T = Al, Si) bonds, and indicates polymerization of the Si–O network [52]. The Si/Al ratio in the AAFs indicates the exact position of the band, although the extent also depends on the type of precursor, reaction time and curing conditions [53]. Changes in wavenumber of the main band are mainly determined by the polymerization/cross-linking of the silica-rich network in C-(N-)A-S-H gel [54,55], which is proposed as the main reaction product in the alkali activation of SW using sodium silicate [28]. It has been stated that the incorporation of H_2O_2 does not alter the alkali activation rate [21]; the position of the band, however, shows slight differences in the polymerization of the foamed material. Since the same amount of stabilising agent is present in all samples, the only difference is in the amount of H_2O_2. Considering the amount of H_2O_2 added, the main Si-O-T asymmetric stretching band is positioned at similar wavenumbers in all samples, except for sample F3, which is positioned at slightly lower wavenumbers (964 cm^{-1}). After 28 days the position of the bands increases slightly compared to after 3 days in all samples except F1, indicating no drastic progression in the polymerization of aluminosilicates. Slight shifts towards higher wavenumbers in F4 and F5 correspond to higher Si/Al ratios, with more Si-O-Si bonds present compared to samples F1–F3. Additionally, lower Ca/Si values (SEM-EDXS Table 4) indicate the position of the band at higher wavenumbers [43,52], as observed in samples F4 and F5. The peaks between 430 and 450 cm^{-1} present in all samples are associated with in-plane bending vibrations of Si–O–Si and O–Si–O [56,57]. Bands for the symmetric stretching of Al–O in Si (Al^{IV})–O–Al^{IV} linkages are positioned between 676 and 684 cm^{-1} in all the foamed materials. After 28 days, samples F2–F5 show bands in the range 1430–1450 cm^{-1}, assigned to the asymmetric stretching vibrations of C-O-C bonds in CO_3^{2-}, and a weak shoulder at approximately 880 cm^{-1}, which is due to out-of-plane bending. These two barely visible bands also appeared after 3 days of curing. The peaks become intensive with ageing, especially in samples F4 and F5. This indicates the carbonation on the matrix during the process, due to the exposure to air, where atmospheric CO_2 reacts with the excess alkali to form Na_2CO_3 (efflorescence phenomena) [39,58,59]. SEM pictures and MIP analysis (described later in the text) confirmed that the F4 and F5 foams contained larger pores, some of which were interconnected. Due to the more porous structure, the conditions are favourable for carbonation and the formation of thermonatrite, as was indicated in samples F3–F5 (Fig. 6). Since the pores are connected in samples F4 and F5, it is suggested that open porosity facilitates the penetration of CO_2 into the internal structure of the specimens. The consumption of sodium resulted in an increased formation of crystal observed as efflorescence, which increased with the amount of foaming agent [12]. Small peaks found by the XRD results matched the peaks of (thermo)natrite, which was quantified by Rietveld refinement. The detection limit of both methods (FTIR and XRD) with respect to the free sodium carbonate (natrite) seems to be similar [60]. The presence of other carbonates in the samples, e.g. dolomite or magnesite, may interfere with the main band of thermonatrite minerals. There were, however, no other carbonates in the AAMs prepared.

Different gels may be formed during alkali activation, either N-A-S-H or C-A-S-H or a combination of the two e.g. C-(N-)A-S-H (high calcium content N-A-S-H gels) [61,62], depending on the precursor used. The chemical composition of SW differs from FA and slag (but it is closer to GGBFS), and N-A-S-H and C-A-S-H gels are not the proposed option, but rather a mixture of both [63]. The main band associated with the asymmetrical stretching vibrations of Si–O bonds (Si–O–Si) in C-A-S-H gel is typically located at around 960 cm^{-1}, while N-A-S-H gels show broader asymmetrical vibration T–O bands (T = Al, Si), which appear at higher wavenumbers (1060 cm^{-1}). The N-A-S-H gel is more porous and may carbonate with an alkaline pore solution (without altering the nanostructure), while the less porous C-A-S-H type gel has a slower carbonation affecting structural alteration during decalcification [64]. In our case, broad bands are positioned in between the typical frequencies for N-A-S-H and C-A-S-H gels. According to the ratios obtained by SEM-EDS (Si/Al, Si/Na, Ca/Si, Na/Al), the matrix formed corresponds to (C,N)-A-S-H gel [61]. As proven in the study by Yliniemi et al., AAMs made of SW have X-ray amorphous C-(N-)A-S-H type gel, which displays greater disorder and a lower Ca content compared to C-A-S-H gel [28]. This is in agreement with the formation of asymmetric stretching vibrations of C-O-C bonds in CO_3^{2-}, and the weak shoulder at around 880 cm^{-1}, which is more intensive in the case of the more porous structures of F4 and F5 and that is favourable in N-A-S-H gel. Although N-A-S-H gel has been proposed in addition to the C-(N-)A-S-H gel

predominant in the matrix, the shifts in the present work do not agree with it, confirming the consumption of Al in the C-(N-)A-S-H gel and thus an excess of Na that can be observed as thermonatrite. N-A-S-H could form in the presence of Ca, but it is only stable at lower pH (< 12) [61] and due to the high pH of alkali activator used in the present work, this is less likely. However, additional studies are needed to confirm this.

3.6. Mercury intrusion porosimetry (MIP)

The results of MIP analyses are shown in Fig. 8. In general, by MIP analyses minimum pore diameter of 5 nm till 1 mm could be measured, whereas artificial air pores with larger sizes, cannot be characterized by this method [65]. However, the pore size distributions in the present work range between 0.003 and 339 μm. The results mainly represent the accessible small pores resulting from the alkali activation of the SW and the macropores induced by the foaming process. According to the literature, the pore structure in AAFs is usually closed. MIP analysis is therefore generally limited, since at low pressure it is unable to reach closed pores, while at high pressure it will break the cell between the pores [66]. Micro-computed tomography (μ-CT), optical microscopy and SEM are commonly used as supplementary methods to MIP analysis [17], and the latter two were used in the present work, as can be seen in Figs. 4 and 5. In order to compare the porosity between samples, MIP analysis was performed on samples F1–F5 after 28 days of curing, where the first 3 days took place at 70 °C followed by room temperature until 28 days.

The results show a wide and scattered pore size distribution in all foams (F1–F5), with an increasing number of pores and pore size as a consequence of the greater addition of H_2O_2. The porosity measured by MIP ranges between 36.5 and 63.2%. Sample F1, to which 1 wt% of foaming agent was added, shows the lowest porosity, while the F5 sample has the highest porosity, at 63.2%. The higher porosity in the alkali-activated matrix may result from a higher amount of foaming agent, a higher alkali activator concentration, and/or a higher temperature [67]. The F1 and F2 samples show a similar porosity, while a significant increase to 55.5% was observed in the F3 samples, as shown in Fig. 8. This is consistent with observations using SEM and an optical microscope. The addition of 2% H_2O_2 seems to be the amount that considerably increases foaming in the AAF when using 1.5 wt% stabilising agent. The proportion of pores sized between 10 and 100 μm increased in samples F3–F5, which was not observed in the samples containing a lower amount of H_2O_2 (samples F1 and F2). Additionally,

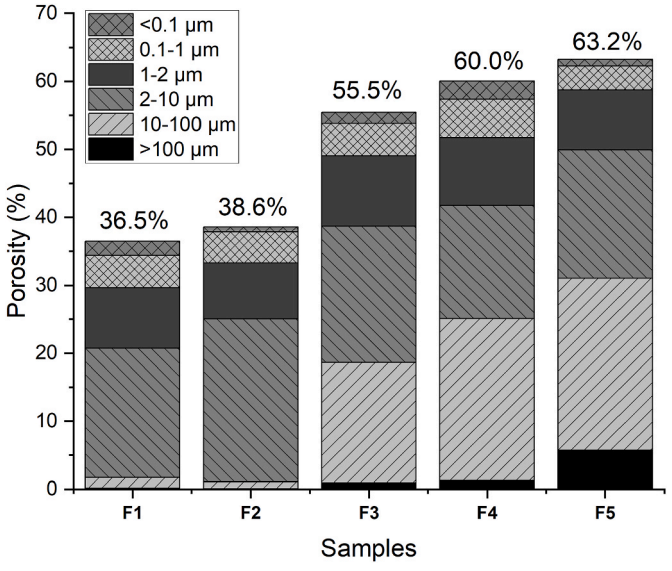

Fig. 8. Pore size distribution in samples F1–F5 prepared using 1–3 wt% H_2O_2 as the foaming agent and 1.5% Triton as the stabilising agent.

the presence of pores bigger than 100 μm is observed in F5. Overall, the proportion of smaller pores (< 0.1, 0.1–1, 1–2 and 2–10 μm) is similar across all samples.

The mechanical properties are weak due to the large pore size distribution (0.5–3.0 mm) formed as a result of the chemical reactions which took place during alkali activation. Larger pores are formed as O_2 is released during the decomposition of H_2O_2. This reaction is catalysed by high pH values and high temperatures [68]. If the size of the bubble released can be controlled, the mechanical properties will be improved [69]. The slow release of gas formed may induce the formation of small, uniform pore-size distributions by adding a stabiliser in the mixture [21]. Incorporating H_2O_2 does not alter the alkali activation rate [21]. The amount of H_2O_2, however, affects the final properties of the AAFs and the amount of swelling, apparent density, pore size, and homogeneity [68]. The chosen surfactant (stabilising agent) influences the size, morphology and topology of the microporous network, but has no impact on the setting time of the mixture [68]. The volume expansion is a consequence of the production of oxygen, and the varying chemical nature of the surfactants added to stabilise the gas bubbles may drastically modify the rheological and interfacial properties of the foams [68]. In this work, the same amount of stabilising agent was used in all samples in order to evaluate the effect of the foaming agent added. By using 2, 2.5 and 3% of H_2O_2, its efficacy is clearly seen.

Mechanical properties depend mainly on the porosity of the structure (Fig. 2), which is a consequence of the H_2O_2 and stabilising agent added, but can also depend on the parameters of the aluminosilicate matrix (influence of Si:Al ratio, influence of other elements [70–72]), on the hardness of the filler (in the present study this represents unreacted particles of SW), on the distribution of the filler "particles" and their size and shape (elongated filler particles can additionally enhance bending strength) in the AAM. The larger the particles, the lower the mechanical strength [31], and if they are not uniformly distributed, there are parts in AAM, which represent stronger or weaker point, just like when pores are not uniformly distributed, regardless of their shape. Table 5 shows a comparison of the values of compressive and bending strength in samples F1–F5, measured after 28 days. Bending strength was lower than compressive strength in F1, whereas these values were similar in F2, and in F3–F5 samples bending strength was greater than compressive strength. This is a consequence of unreacted elongated particles, which

Table 5
Comparison of average compressive and bending strengths, total intrusion volume, average pore diameter, and densities obtained by MIP bulk and skeletal), pycnometer (true density) and measured with calipers (geometrical density). All the results represent values after 28 days curing (3 days curing at 70 °C followed by 25 days curing at room temperature).

	F1	F2	F3	F4	F5
Average compressive strengths (MPa)	12.62	7.47	3.10	2.11	1.47
Standard deviation of measurements (MPa)	0.60	0.65	0.31	0.18	0.14
Average bending strengths (MPa)	6.35	6.08	3.99	2.87	1.73
Standard deviation of measurements (MPa)	0.43	0.1	0.41	0.29	0.28
Total intrusion volume (mL/g)	0.26	0.30	0.53	0.63	0.80
Average pore diameter (μm)	0.07	0.21	0.48	0.38	1.44
Bulk density (g/cm^3)	1.40	1.30	1.04	0.95	0.79
True density measured by pycnometer (g/cm^3)	2.33 ± 0.00	2.37 ± 0.00	2.44 ± 0.01	2.44 ± 0.04	2.52 ± 0.05
Geometrical density (g/cm^3)	1.44 ± 0.04	1.26 ± 0.03	0.90 ± 0.03	0.67 ± 0.02	0.54 ± 0.02
Skeletal density (g/cm^3)	2.23	2.12	2.37	2.31	2.27
Porosity (%) obtained by MIP	36.5 ± 0.7	38.6 ± 1.0	55.5 ± 1.5	60.0 ± 1.9	63.2 ± 2.8
Total porosity (%) (calculated)	37.8 ± 1.0	46.8 ± 1.3	63.0 ± 2.2	72.5 ± 3.4	78.6 ± 4.0

do not dissolve and with getting incorporated into aluminosilicate structure contribute to the final mechanical properties. The more porous the structure (the higher the number of pores/cracks), the greater the number of interconnected pores, the thinner the walls between the pores (the walls are the ones that carry the load, and their shape and thickness affect the transfer of the applied external forces), the greater is the effect on reducing the mechanical strength and geometrical density. In our previous study the porosities of non-foamed AAMs prepared of SW were in the range 25–32% [27] that is less than in F1 sample. This confirmed the influence of foaming agent even with the addition of only 1 wt% of H_2O_2. Table 5 shows the values for total intrusion volume, average pore diameter and the various densities. Bulk (obtained by MIP) and geometrical (measured by calipers) densities both decrease, while porosity increases. On the other hand, the skeletal density of foams F1–F5 is similar for all of them (Table 5, varying in the range between 2.12 and 2.37 g/cm^3), which is predicted because the mixture of ingredients contributing to the alkali activation is the same and varies only by the addition of foaming agents and stabilisers, which affect only the geometrical density, i.e., the porosity and, consequently, the mechanical strengths. In present work, focus was not put on the influence of the stabiliser on the mechanical strengths, but according to our previous work [37], it was found out that the mechanical strength decreased when the amount of stabiliser was too high, whereas too low amount of stabiliser did not stabilise the gas bubbles well enough and many of them escaped from the interstices of the forming aluminosilicate matrix.

Since the MIP can only achieve open and smaller pores, the total porosity was determined by measurements with the pycnometer. Total porosity (Φ) was calculated using the geometrical (ρ_g) and true densities (ρ_T), based on the following equation:

$$\boldsymbol{\Phi} = 1 - \frac{\boldsymbol{\rho_g}}{\boldsymbol{\rho_T}}$$

The total intrusion volume and bulk density were similar in samples F1 and F2, while the average pore diameter was lower compared to F3–F5. The coarsening of the microstructure in all the foams is characterised by increases in the total intrusion volume, average pore diameter and total porosity, while the bulk density decreases. As expected, total porosity is higher than the porosity obtained by MIP, ranging between 37.8 and 78.6% since closed pores and bigger pores that cannot be identified by MIP analyses (bigger than 339 μm) are included. SEM micrographs and images obtained by optical microscope confirm the presence of bigger pores that could not be measured by MIP (> 340 μm). As observed in Fig. 8, the proportion of pores sized between 10 and 100 μm and > 100 μm increases in F1–F5 samples, while the proportion of pores of other sizes is similar across all samples. These smaller voids are seen in the SEM pictures, where the size of micro-cracks decreases as the amount of H_2O_2 added, and thus porosity, increased. Our previous study observed that introducing additional water into SW samples accelerated the formation of smaller pores [27]. In this work, additional water was added to the AAM, while a small part also arises due to the decomposition of H_2O_2. Voids (small micro-cracks) may also, however, form in the matrix due to the partial evaporation of excess water during the thermal curing of the specimens.

3.7. Thermal conductivity

Additional experiments were performed to estimate the thermal conductivity in the F1–F5 foams, the results of which are presented in Table 6. The thermal conductivity of the least porous sample (F1) was 0.157 W W/(m·K), falling to 0.092 W/(m·K) for the most porous one (F5), with the range of apparent densities for the corresponding samples being 1.31–0.74 g/cm^3. Total porosity increase with decreasing density as could be seen in Table 6. The amount of porosity should be in the range of 50–95% to achieve lightweight and thermal insulating properties [73].

Aerated concrete containing 50–80% or more of air bubbles, voids, and capillary porosity [74], whose final properties, such as density, mechanical strength, and thermal and acoustic conductivity, depend on curing conditions and the varying compositions of the initial cement slurry [75]. Due to appropriate manufacturing processes, the density of aerated concrete (0.3–1.8 g/cm^3) varies depending on the application [76]. Typical values of thermal conductivity and compressive strength in common thermal insulating materials range between 0.030 and 0.230 W/(m·K) and 0.04–1.5 MPa, respectively [77]. Thermal conductivity values for fire-resistant AAM are in the range 0.1–0.3 W/(m·K), which is relatively low in comparison to the other commonly used structural building materials and almost identical or comparable to the marketable fire-resistant materials [78] while foamed material intended for insulation use should be close to 0.070 W/(m·K) [79]. More detailed comparison of various materials typically used for insulation purposes and AAF mainly prepared by H_2O_2 as a foaming agent are presented in Table 7.

Table 6
Density and thermal conductivity of AAFs (F1–F5) following 3 days curing at 70 °C.

	Geometrical density (g/cm^3)	Porosity (%)	Thermal conductivity (W/(m·K))
F1	1.31	37.8	0.157
F2	1.22	46.8	0.151
F3	1.06	63.0	0.123
F4	0.78	72.5	0.093
F5	0.74	78.6	0.092

The foamed waste mineral wool samples obtained in the present work have porosities > 36% and a thermal conductivity coefficient lower than < 0.16 W/(m·K). In comparison to other studies using SW or GW in the AAFs (bolded data in Table 7), our thermal conductivity is the lowest although the density is higher [11,13]. However, compressive strength is lower compared to the AAF produced by Erofeev et al. and Kozub et al. [11,13] but higher than in the study of Alzaza et al. where they used premade foam [12]. Our AAFs cannot be compared with the commonly used insulation material such as polyurethane foams, SW etc., due to their significantly lower thermal conductivities and densities. In general, AAF prepared in this study are comparable with foamed concrete and autoclaved aerated concrete s (AAC) showing lower thermal conductivity and compressive strength than AAC at higher density. On the other hand, bending strength of SW AAF is better than with AAC as shown in Table 7. Comparison with other AAF prepared of FA, metakaolin, slags show similar thermal conductivities, while densities are mostly lower than foamed SW as well as compressive strengths. The improved mechanical properties achieved by decreasing the thermal conductivity indicate the suitability of the material for thermal-insulation applications that do not demand a high load-bearing capacity.

The pore volume fraction controls the thermal conductivity, as the most porous sample exhibits the lowest thermal conductivity [89]. Porosities of AAFs from other studies presented in Table 7 range between 51.4 and 86.5% (not all data were available). The total porosity of F5 sample is 78.6% which is among the highest considering other studies. However, in the study of Bai et al. where the highest porosity was achieved (86.5%), the thermal conductivity was 0.091 W/(m·K) similar as in our work even the density was much lower than in our study. In the study of Kozub et al., where the porosity reach 51.4% at 0.50 g/cm^3, the thermal conductivity was 0.113 W/(m·K) [13]. Thermal conductivity depends on the structure of the material, in terms of its pore distribution, morphology, pore volume and the nature of the gas filling the pores [90]. A higher porosity with more pores resulted in the lowering of the material's thermal conductivity, because the thermal conductivity of air within the pores is much lower than that of a solid substance [85], as is consistent with the present work. The development of homogenous porosity is related to the workability of the initial material [91,92], and resulted in the material having a lower thermal conductivity. For low

Table 7
Thermal conductivities, apparent densities, porosities and compressive strengths of different thermal insulation products. Some values are missing because they are not available or authors did not provide them. Thermal insulation product are divided into three parts (different colours in the table), most commonly used insulation materials (light blue), AAFs using H_2O_2 as a foaming agent (grey colour) and in the last group (pink colour) there are materials where mineral wool waste is used in the foamed mixture [80–84,86–88].

AAF and precursors, foaming and stabilising agents used	Thermal conductivity (W/(m·K))	Alkali activator used in the study	Apparent density (g/cm^3)	Porosity (%)	Compressive strength (MPa)	Reference
Polyurethane foam	0.026	/	0.035-0.050	/	0.1-0.5	[1,80,81]
Extruded polystyrene foam	0.025-0.035	/	0.020-0.080	/	0.15-0.7	[1,80,81]
Stone wool	0.033–0.045	/	0.020-0.200	/	0.015-0.08	[81,82]
Glass wool	0.030–0.045	/	0.020-0.200	/	0.015-0.08	[1,81,82]
Foamed concrete	0.10–0.11	/	0.400-0.600	/	0.5-1.5	[83]
Autoclaved aerated concrete	0.12-0.20	/	0.450-0.750	/	3.2-7.5 0.65-1.25*	[83]
Foamy perlite AAF (2 wt% of H_2O_2)	0.03	8M NaOH	0.290	/	0.78	[41]
Foamy perlite AAF (0.25 wt% of H_2O_2)	0.076 (2M NaOH) 0.095 (4M NaOH)	2M and 4M NaOH	0.408–0.477	72.0 at 2M NaOH	< 1	[84]
FA AAF (0.3 wt% H_2O_2, 1 wt% surfactant)			0.940	73.0	1.7	[22]
MK-WG AAF (3 wt% H_2O_2, 3 wt% Triton-X100)	0.210	11M KOH mixed with potassium silicate	0.920	/	7.3	[58]
FA AAF	0.072	Sodium silicate	0.239	81.2	0.67	[85]
FA AAF (0.5 wt% H_2O_2)	/		0.610		2.9	[86]
FA AAF (1.2 wt% H_2O_2)	0.107	Sodium silicate + 12M NaOH	0.560	72.5	1.23	[87]
FA AAF (5 wt% of H_2O_2, 1.0wt% sodium dodecyl benzene sulfonate and 0.8 wt% triethanolamine)	/	Sodium silicate + NaOH	0.277	63.0	0.65	[23]
MK and GGBFS (2 wt% H_2O_2, 0.05 wt% surfactant)	0.084	Sodium silicate + NaOH	0.264	/	0.53	[16]
MK (15 wt% H_2O_2 and 3.75 wt% Tween80)	0.091	11M KOH + potassium silicate	0.300	86.5	0.3	[19]
FA AAF (7 wt% H_2O_2 + Microspheres)	0.095	Sodium silicate + 14M NaOH	0.402	/	1.9	[88]
FA AAF (3 wt% H_2O_2)	0.082	8M NaOH	0.440	80.9	/	[21]
SW AAF (3 wt% H_2O_2, 1.5 wt% Triton)	**0.092**	**Sodium silicate**	**0.740**	**78.6**	**1.47 1.73***	**Our study**
Mineral wool production waste (0.06-1.2 wt% Al-powder)	**0.144**	**1.5-3 wt% NaOH**	**0.610**	/	**1.7**	[11]
GW (5 wt%), FA (47.5 wt%) sand (47.5 wt%) (3 wt% H_2O_2 and 0.5 wt% Al-powder)	**0.113**	**Sodium silicate, modul 2.5 + 10M NaOH**	**0.500**	**51.4**	**3.43**	[13]
SW/GW (weight ratios of 5 and 1), MK (40 wt%), sand and PP (35 wt% premade foams from protein-based foaming agent)	/	**Sodium silicate, modul 2.5 + 10M NaOH**	**0.770**	/	**1.00**	[12]

*Bending strength MK=metakaolin, GGBFS=ground granulated blast furnace slag, WG=waste glass, PP=polypropylene fibers

thermal conductivity, the presence of high ultra-macroporosity, roundness, the dimension of the pores, and a reduction in interpore partition thickness are also important [93]. Interpore space is, therefore, reduced and more heat is accumulated [94]. In our study, by adding water to the mixture, basicity reduced slightly, and workability improved, which affects the viscosity of the paste. The present work shows that the irregular pore size distributions and the pore coalescence observed as interconnected pores in F4 and F5 decrease the thermal conductivity of the samples. Since SW fibres vary in size, larger fibres may affect as fine aggregate, which could explain the low thermal conductivity, as well as the density achieved [11,95].

4. Conclusions

Foamed AAM are a promising alternative to other foamed materials. The present research confirms that AAFs produced from waste stone wool have good mechanical properties and performance in comparison to the typical construction product. Hydrogen peroxide (H_2O_2) and Triton are suitable foaming and stabilising agents leading to randomly distributed pores of different sizes. 1 wt% to 3 wt% H_2O_2, and 1.5 wt% stabilising agent was used in all experiments. The amount of H_2O_2 added influences the density and mechanical properties of the final material. By properly mixing and adding the foaming and stabilising agents it is possible to obtain foamed materials with a density between 0.5 and 0.8 g/cm^3. Adding a greater amount of H_2O_2 led to the material having a lower density, lower compressive strength, and higher porosity (up to 79%). High porosity foams (F4 and F5) include many interconnected pores which decrease the thermal conductivity of the samples to 0.092 W/(m·K), with densities below 0.8 g/cm^3. The results prove that waste mineral wool could be a suitable precursor for foamed AAM, and that foams produced in this way can be used as insulation materials in construction. However, further studies need to be conducted in the future, including various durability tests (capillary water absorption, water vapour permeability, freeze-thaw test, and eventually also fire resistance test, etc.) to confirm the suitability of this type of insulation material. Further attempts in lowering density should be also made in order to be competitive to the highly insulation products (as the ones listed in first part of Table 7). Since a lot of mineral wool ends up in landfills, the influence of other types of wool (e.g. GW) on mechanical properties and porosity should be studied. In addition, the fibrous structure of the material and the milling of the mineral wool itself can significantly affect the final properties of the material, and this will also be a focus of our next step. Given the large amount of mineral wool waste generated and the target that 70% of non-hazardous C&D waste must be prepared for reuse, recycling or recovery by 2020 (stated by European Union legislation), there is an urgent need to increase the reuse and recycling of mineral wool waste and various application options should be tested.

Declaration of competing interest

The authors declare that they have no known competing financial interests or personal relationships that could have appeared to influence the work reported in this paper.

Acknowledgement

H2020 project Wool2Loop has received funding from the European Union's Horizon 2020 research and innovation programme under grant agreement No. 821000. The opinions expressed in this document only reflect the authors' view and in no way reflect the European Commission's opinions. The European Commission is not responsible for any use that may be made of the information it contains.

The Metrology Institute of the Republic of Slovenia is acknowledged for the use of XRF.

References

[1] A.M. Papadopoulos, State of the art in thermal insulation materials and aims for future developments, Energy Build. 37 (2005) 77–86, https://doi.org/10.1016/j.enbuild.2004.05.006.

[2] O. Väntsi, T. Kärki, Mineral wool waste in Europe: a review of mineral wool waste quantity, quality, and current recycling methods, J. Mater. Cycles Waste Manag. 16 (2014) 62–72, https://doi.org/10.1007/s10163-013-0170-5.

[3] T. Sattler, R. Pomberger, J. Schimek, D. Vollprecht, Mineral Wool Waste in Austria, Associated Health Aspects and Recycling Options, 2020, p. 174. Detritus.

[4] A. Müller, B. Leydolph, K. Stanelle, Recycling mineral wool waste: technologies for the conversion of the fiber structure, Part 1, Interceram 58 (2009) 378–381.

[5] R. Ji, Y. Zheng, Z. Zou, Z. Chen, S. Wei, X. Jin, M. Zhang, Utilization of mineral wool waste and waste glass for synthesis of foam glass at low temperature, Construct. Build. Mater. 215 (2019) 623–632, https://doi.org/10.1016/j.conbuildmat.2019.04.226.

[6] Z. Chen, H. Wang, R. Ji, L. Liu, C. Cheeseman, X. Wang, Reuse of mineral wool waste and recycled glass in ceramic foams, Ceram. Int. 45 (2019) 15057–15064, https://doi.org/10.1016/j.ceramint.2019.04.242.

[7] J. König, A. Lopez-Gil, P. Cimavilla-Roman, M.A. Rodriguez-Perez, R.R. Petersen, M.B. Østergaard, N. Iversen, Y. Yue, M. Spreitzer, Synthesis and properties of open- and closed-porous foamed glass with a low density, Construct. Build. Mater. 247 (2020) 118574.

[8] V. Ducman, A. Mladenovič, J.S. Šuput, Lightweight aggregate based on waste glass and its alkali–silica reactivity, Cement Concr. Res. 32 (2002) 223–226.

[9] L. Korat, V. Ducman, Characterization of fly ash alkali activated foams obtained using sodium perborate monohydrate as a foaming agent at room and elevated temperatures, Front. Mater. 7 (2020) 308.

[10] K. Traven, M. Češnovar, S.D. Škapin, V. Ducman, High temperature resistant fly-ash and metakaolin-based alkali-activated foams, Ceram. Int. (2021), https://doi.org/10.1016/j.ceramint.2021.05.241.

[11] V.T. Erofeev, A.I. Rodin, V.S. Bochkin, V. V Yakunin, A.A. Ermakov, Lightweight geopolymers made of mineral wool production waste, ИнЖенерно-Строительный Журнал (2020) 3–12.

[12] A. Alzaza, M. Mastali, P. Kinnunen, L. Korat, Z. Abdollahnejad, V. Ducman, M. Illikainen, Production of lightweight Alkali activated mortars using mineral wools, Materials 12 (2019) 1695, https://doi.org/10.3390/ma12101695.

[13] B. Kozub, P. Bazan, R. Gailitis, K. Korniejenko, D. Mierzwiński, Foamed geopolymer composites with the addition of glass wool waste, Materials 14 (2021) 4978.

[14] M. Mastali, P. Kinnunen, H. Isomoisio, M. Karhu, M. Illikainen, Mechanical and acoustic properties of fiber-reinforced alkali-activated slag foam concretes containing lightweight structural aggregates, Construct. Build. Mater. 187 (2018) 371–381, https://doi.org/10.1016/j.conbuildmat.2018.07.228.

[15] S.T. Erdoğan, Inexpensive intumescent alkali-activated natural pozzolan pastes, J. Eur. Ceram. Soc. 35 (2015) 2663–2670, https://doi.org/10.1016/j.jeurceramsoc.2015.03.017.

[16] G. Samson, M. Cyr, X.X. Gao, Thermomechanical performance of blended metakaolin-GGBS alkali-activated foam concrete, Construct. Build. Mater. 157 (2017) 982–993, https://doi.org/10.1016/j.conbuildmat.2017.09.146.

[17] L. Korat, V. Ducman, The influence of the stabilizing agent SDS on porosity development in alkali-activated fly-ash based foams, Cement Concr. Compos. 80 (2017) 168–174, https://doi.org/10.1016/j.cemconcomp.2017.03.010.

[18] Y. Liu, C. Yan, Z. Zhang, Y. Gong, H. Wang, X. Qiu, A facile method for preparation of floatable and permeable fly ash-based geopolymer block, Mater. Lett. 185 (2016) 370–373, https://doi.org/10.1016/j.matlet.2016.09.044.

[19] C. Bai, G. Franchin, H. Elsayed, A. Zaggia, L. Conte, H. Li, P. Colombo, High-porosity geopolymer foams with tailored porosity for thermal insulation and wastewater treatment, J. Mater. Res. 32 (2017) 3251–3259, https://doi.org/10.1557/jmr.2017.127.

[20] A.N. Murri, V. Medri, E. Papa, L. Laghi, C. Mingazzini, E. Landi, Porous geopolymer insulating core from a metakaolin/biomass ash composite, Environments (2017) 4.

[21] R.M. Novais, G. Ascensão, L.H. Buruberri, L. Senff, J.A. Labrincha, Influence of blowing agent on the fresh- and hardened-state properties of lightweight geopolymers, Mater. Des. 108 (2016) 551–559, https://doi.org/10.1016/j.matdes.2016.07.039.

[22] G. Masi, W.D.A. Rickard, L. Vickers, M.C. Bignozzi, A. van Riessen, A comparison between different foaming methods for the synthesis of light weight geopolymers, Ceram. Int. 40 (2014) 13891–13902, https://doi.org/10.1016/j.ceramint.2014.05.108.

[23] Z. Liu, N. Shao, D. Wang, J. Qin, T. Huang, W. Song, M. Lin, J. Yuan, Z. Wang, Fabrication and properties of foam geopolymer using circulating fluidized bed combustion fly ash, Int. J. Miner. Metall. Mater. 21 (2014) 89–94, https://doi.org/10.1007/s12613-014-0870-4.

[24] S.F.A. Zaidi, E. Ul Haq, K. Nur, N. Ejaz, M. Anis-ur-Rehman, M. Zubair, M. Naveed, Synthesis & characterization of natural soil based inorganic polymer foam for thermal insulations, Construct. Build. Mater. 157 (2017) 994–1000, https://doi.org/10.1016/j.conbuildmat.2017.09.112.

[25] Z. Zhang, J.L. Provis, A. Reid, H. Wang, Geopolymer foam concrete: an emerging material for sustainable construction, Construct. Build. Mater. 56 (2014) 113–127, https://doi.org/10.1016/j.conbuildmat.2014.01.081.

[26] C. Bai, T. Ni, Q. Wang, H. Li, P. Colombo, Porosity, mechanical and insulating properties of geopolymer foams using vegetable oil as the stabilizing agent, J. Eur. Ceram. Soc. 38 (2018) 799–805, https://doi.org/10.1016/j.jeurceramsoc.2017.09.021.

[27] M. Pavlin, B. Horvat, A. Frankovič, V. Ducman, Mechanical, microstructural and mineralogical evaluation of alkali-activated waste glass and stone wool, Ceram. Int. (2021), https://doi.org/10.1016/j.ceramint.2021.02.068.

[28] J. Yliniemi, B. Walkley, J.L. Provis, P. Kinnunen, M. Illikainen, Nanostructural evolution of alkali-activated mineral wools, Cement Concr. Compos. 106 (2020) 103472, https://doi.org/10.1016/J.CEMCONCOMP.2019.103472.

[29] J. Yliniemi, P. Kinnunen, P. Karinkanta, M. Illikainen, Utilization of mineral wools as alkali-activated material precursor, Materials 9 (2016) 312, https://doi.org/10.3390/ma9050312.

[30] K. Traven, M. Češnovar, V. Ducman, Particle size manipulation as an influential parameter in the development of mechanical properties in electric arc furnace slag-based AAM, Ceram. Int. 45 (2019) 22632–22641, https://doi.org/10.1016/j.ceramint.2019.07.296.

[31] B. Horvat, V. Ducman, Influence of particle size on compressive strength of alkali activated refractory materials, Materials 13 (2020) 2227.

[32] M. Pavlin, B. Horvat, V. Ducman, Challenges at upscaling from laboratory to industrial level in Wool2Loop project, in: Technol. Bus. Model. Circ. Econ, 2021,

p. 35. Portorož (Slovenia), http://tbmce.um.si/wp-content/uploads/2021/09/02_TBMCE2021_Book_of_Abstracts.pdf.
[33] P. Perumal, T. Luukkonen, H. Sreenivasan, P. Kinnunen, M. Illikainen, in: C. E. Chaudhary (Ed.), 15 - Porous Alkali-Activated Materials, Butterworth-Heinemann, 2020, pp. 529–563, https://doi.org/10.1016/B978-0-12-818961-0.00015-6. P. Samui, D. Kim, N.R. Iyer, S.B.T.-N.M.
[34] M. Pavlin, A. Frankovič, B. Horvat, V. Ducman, Early strength improvement of waste wool based alkali activated material, in: B. Abstr. 74th RILEM Annu. Week 40th Cem. Concr. Sci. Conf, The University of Sheffield, Sheffield, United Kingdom, 2020, p. 259. https://www.sheffield.ac.uk/materials/rilem2020/programme.
[35] M. Češnovar, K. Traven, B. Horvat, V. Ducman, The potential of ladle slag and electric arc furnace slag use in synthesizing alkali activated materials; the influence of curing on mechanical properties, Materials 12 (2019) 1173.
[36] K. Traven, M. Češnovar, V. Ducman, Suitability of different stabilizing agents in alkali-activated fly-ash based foams, in: RILEM Spring Conv. Conf, Springer, 2020, pp. 155–164.
[37] B. Horvat, V. Ducman, Potential of green ceramics waste for alkali activated foams, Materials 12 (2019) 3563.
[38] P. Duxson, J.L. Provis, G.C. Lukey, S.W. Mallicoat, W.M. Kriven, J.S.J. van Deventer, Understanding the relationship between geopolymer composition, microstructure and mechanical properties, Colloids Surfaces A Physicochem. Eng. Asp. 269 (2005) 47–58, https://doi.org/10.1016/J.COLSURFA.2005.06.060.
[39] V.F.F. Barbosa, K.J.D. MacKenzie, C. Thaumaturgo, Synthesis and characterisation of materials based on inorganic polymers of alumina and silica: sodium polysialate polymers, Int. J. Inorg. Mater. 2 (2000) 309–317, https://doi.org/10.1016/S1466-6049(00)00041-6.
[40] J. Davidovits, Geopolymers: inorganic polymeric new materials, J. Therm. Anal. Calorim. 37 (1991) 1633–1656.
[41] V. Vaou, D. Panias, Thermal insulating foamy geopolymers from perlite, Miner. Eng. 23 (2010) 1146–1151, https://doi.org/10.1016/j.mineng.2010.07.015.
[42] E. Najafi Kani, A. Allahverdi, J.L. Provis, Efflorescence control in geopolymer binders based on natural pozzolan, Cement Concr. Compos. 34 (2012) 25–33, https://doi.org/10.1016/j.cemconcomp.2011.07.007.
[43] A. Fernández-Jiménez, F. Puertas, Effect of activator mix on the hydration and strength behaviour of alkali-activated slag cements, Adv. Cement Res. 15 (2003) 129–136, https://doi.org/10.1680/adcr.2003.15.3.129.
[44] C. Shi, R.L. Day, Selectivity of alkaline activators for the activation of slags, Cem. Concr. Aggregates 18 (1996) 8–14.
[45] K. König, K. Traven, M. Pavlin, V. Ducman, Evaluation of locally available amorphous waste materials as a source for alternative alkali activators, Ceram. Int. (2020), https://doi.org/10.1016/j.ceramint.2020.10.059.
[46] Z. Zhang, J.L. Provis, X. Ma, A. Reid, H. Wang, Efflorescence and subflorescence induced microstructural and mechanical evolution in fly ash-based geopolymers, Cement Concr. Compos. 92 (2018) 165–177.
[47] C. Dow, F.P. Glasser, Calcium carbonate efflorescence on Portland cement and building materials, Cement Concr. Res. 33 (2003) 147–154.
[48] Z. Zhang, J.L. Provis, A. Reid, H. Wang, Fly ash-based geopolymers: the relationship between composition, pore structure and efflorescence, Cement Concr. Res. 64 (2014) 30–41.
[49] M.R. Rowles, J. V Hanna, K.J. Pike, M.E. Smith, B.H. O'connor, 29 Si, 27 Al, 1 H and 23 Na MAS NMR study of the bonding character in aluminosilicate inorganic polymers, Appl. Magn. Reson. 32 (2007) 663–689.
[50] J.L. Bass, G.L. Turner, Anion distributions in sodium silicate solutions. Characterization by 29Si NMR and infrared spectroscopies, and vapor phase osmometry, J. Phys. Chem. B 101 (1997) 10638–10644.
[51] C.A. Rees, Mechanisms and Kinetics of Gel Formation in Geopolymers, 2007.
[52] P. Yu, R.J. Kirkpatrick, B. Poe, P.F. McMillan, X. Cong, Structure of calcium silicate hydrate (C-S-H): near-, mid-, and far-infrared spectroscopy, J. Am. Ceram. Soc. 82 (1999) 742–748, https://doi.org/10.1111/j.1151-2916.1999.tb01826.x.
[53] O. Rudić, V. Ducman, M. Malešev, V. Radonjanin, S. Draganić, S. Šupić, M. Radeka, Aggregates obtained by alkali activation of fly ash: the effect of granulation, pelletization methods and curing regimes, Materials 12 (2019) 776, https://doi.org/10.3390/ma12050776.
[54] S. Zhang, Z. Li, B. Ghiassi, S. Yin, G. Ye, Fracture properties and microstructure formation of hardened alkali-activated slag/fly ash pastes, Cement Concr. Res. 144 (2021) 106447.
[55] S. Zhang, A. Keulen, K. Arbi, G. Ye, Waste glass as partial mineral precursor in alkali-activated slag/fly ash system, Cement Concr. Res. 102 (2017) 29–40, https://doi.org/10.1016/j.cemconres.2017.08.012.
[56] Z. Zhang, H. Wang, J.L. Provis, Quantitative study of the reactivity of fly ash in geopolymerization by FTIR, J. Sustain. Cem. Mater. 1 (2012) 154–166.
[57] W.K.W. Lee, J.S.J. van Deventer, Use of infrared spectroscopy to study geopolymerization of heterogeneous amorphous aluminosilicates, Langmuir 19 (2003) 8726–8734, https://doi.org/10.1021/la026127e.
[58] C. Bai, H. Li, E. Bernardo, P. Colombo, Waste-to-resource preparation of glass-containing foams from geopolymers, Ceram. Int. 45 (2019) 7196–7202.
[59] A. Allahverdi, E.N. Kani, K.M.A. Hossain, M. Lachemi, Methods to control efflorescence in alkali-activated cement-based materials, in: Handb. Alkali-Activated Cem. Mortars Concr, Elsevier, 2015, pp. 463–483.
[60] S. Kaufhold, K. Emmerich, R. Dohrmann, A. Steudel, K. Ufer, Comparison of methods for distinguishing sodium carbonate activated from natural sodium bentonites, Appl. Clay Sci. 86 (2013) 23–37, https://doi.org/10.1016/j.clay.2013.09.014.
[61] I. Garcia-Lodeiro, A. Palomo, A. Fernández-Jiménez, D.E. Macphee, Compatibility studies between N-A-S-H and C-A-S-H gels. Study in the ternary diagram Na2O–CaO–Al2O3–SiO2–H2O, Cement Concr. Res. 41 (2011) 923–931, https://doi.org/10.1016/j.cemconres.2011.05.006.
[62] I. García-Lodeiro, A. Fernández-Jiménez, A. Palomo, D.E. Macphee, Effect of calcium additions on N–A–S–H cementitious gels, J. Am. Ceram. Soc. 93 (2010) 1934–1940.
[63] P. Kinnunen, J. Yliniemi, B. Talling, M. Illikainen, Rockwool Waste in Fly Ash Geopolymer Composites, J. Mater. Cycles Waste Manag, 2016, https://doi.org/10.1007/s10163-016-0514-z full text available at: http://rdcu.be/ncgH.
[64] S.A. Bernal, J.L. Provis, B. Walkley, R. San Nicolas, J.D. Gehman, D.G. Brice, A. R. Kilcullen, P. Duxson, J.S.J. van Deventer, Gel nanostructure in alkali-activated binders based on slag and fly ash, and effects of accelerated carbonation, Cement Concr. Res. 53 (2013) 127–144, https://doi.org/10.1016/j.cemconres.2013.06.007.
[65] G. Schober, Porosity in autoclaved aerated concrete (AAC): a review on pore structure, types of porosity, measurement methods and effects of porosity on properties, in: 5th Int. Conf. Autoclaved Aerated Concr, 2011, pp. 351–359. Bydgoscsz Poland.
[66] H. Assaedi, T. Alomayri, F.U.A. Shaikh, I.M. Low, 19 - advances in geopolymer composites with natural reinforcement, in: Woodhead Publ. Ser. Compos. Sci. Eng, Woodhead Publishing, 2018, pp. 461–474, https://doi.org/10.1016/B978-0-08-102166-8.00019-0. I.M.B.T.-A. in C.M.C. (Second E. Low (Ed.).
[67] A. Hajimohammadi, T. Ngo, P. Mendis, T. Nguyen, A. Kashani, J.S.J. van Deventer, Pore characteristics in one-part mix geopolymers foamed by H2O2: the impact of mix design, Mater. Des. 130 (2017) 381–391, https://doi.org/10.1016/j.matdes.2017.05.084.
[68] S. Petlitckaia, A. Poulesquen, Design of lightweight metakaolin based geopolymer foamed with hydrogen peroxide, Ceram. Int. 45 (2019) 1322–1330, https://doi.org/10.1016/j.ceramint.2018.10.021.
[69] T.-Y. Yang, C.-C. Chou, C.-C. Chien, The effects of foaming agents and modifiers on a foamed-geopolymer, in: Adv. Civil, Environ. Mater. Res., Seoul, Korea, 2012.
[70] M. Komljenović, Z. Baščarević, V. Bradić, Mechanical and microstructural properties of alkali-activated fly ash geopolymers, J. Hazard Mater. 181 (2010) 35–42, https://doi.org/10.1016/j.jhazmat.2010.04.064.
[71] P. Duxson, S.W. Mallicoat, G.C. Lukey, W.M. Kriven, J.S.J. van Deventer, The effect of alkali and Si/Al ratio on the development of mechanical properties of metakaolin-based geopolymers, Colloids Surfaces A Physicochem. Eng. Asp. 292 (2007) 8–20, https://doi.org/10.1016/j.colsurfa.2006.05.044.
[72] K. Hrachovcová, Z. Tišler, E. Svobodová, J. Šafář, Modified alkali activated zeolite foams with improved textural and mechanical properties, Miner 10 (2020), https://doi.org/10.3390/min10050483.
[73] V. Medri, E. Papa, J. Dedecek, H. Jirglova, P. Benito, A. Vaccari, E. Landi, Effect of metallic Si addition on polymerization degree of in situ foamed alkali-aluminosilicates, Ceram. Int. 39 (2013) 7657–7668.
[74] M. Scheffler, P. Colombo, Cellular Ceramics: Structure, Manufacturing, Properties and Applications, John Wiley & Sons, 2006.
[75] P.O. Guglielmi, W.R.L. Silva, W.L. Repette, D. Hotza, Porosity and mechanical strength of an autoclaved clayey cellular concrete, Adv. Civ. Eng. 2010 (2010).
[76] N. Narayanan, K. Ramamurthy, Structure and properties of aerated concrete: a review, Cement Concr. Compos. 22 (2000) 321–329.
[77] V.E. Manevich, K.Y. Subbotin, Foam glass and problems of energy conservation, Glas. Ceram. 65 (2008) 105–108.
[78] K. Sakkas, P. Nomikos, A. Sofianos, D. Panias, Utilisation of FeNi-slag for the production of inorganic polymeric materials for construction or for passive fire protection, Waste Biomass Valoriz. 5 (2014) 403–410.
[79] F. Pacheco-Torgal, J. Labrincha, C. Leonelli, A. Palomo, P. Chindaprasit, Handbook of Alkali-Activated Cements, Mortars and Concretes, Elsevier, 2014.
[80] L. Jiang, H. Xiao, W. An, Y. Zhou, J. Sun, Correlation study between flammability and the width of organic thermal insulation materials for building exterior walls, Energy Build. 82 (2014) 243–249.
[81] S. Kowatsch, in: L. Pilato (Ed.), Mineral Wool Insulation Binders BT - Phenolic Resins: A Century of Progress, Springer Berlin Heidelberg, Berlin, Heidelberg, 2010, pp. 209–242, https://doi.org/10.1007/978-3-642-04714-5_10.
[82] L. Ducoulombier, Z. Lafhaj, Comparative study of hygrothermal properties of five thermal insulation materials, Case Stud. Therm. Eng. 10 (2017) 628–640.
[83] A.J. Hamad, Materials, production, properties and application of aerated lightweight concrete, Int. J. Mater. Sci. Eng. 2 (2014) 152–157.
[84] L. Profitis, I. Douni, E. Chatzitheodorides, D. Panias, Development of lightweight insulating building materials from perlite wastes, Mater. Construcción 69 (2019) e175.
[85] J. Feng, R. Zhang, L. Gong, Y. Li, W. Cao, X. Cheng, Development of porous fly ash-based geopolymer with low thermal conductivity, Mater. Des. 65 (2015) 529–533, https://doi.org/10.1016/j.matdes.2014.09.024.
[86] V. Ducman, L. Korat, Characterization of geopolymer fly-ash based foams obtained with the addition of Al powder or H2O2 as foaming agents, Mater. Char. 113 (2016) 207–213.
[87] R.M. Novais, L.H. Buruberri, G. Ascensão, M.P. Seabra, J.A. Labrincha, Porous biomass fly ash-based geopolymers with tailored thermal conductivity, J. Clean. Prod. 119 (2016) 99–107.
[88] M. Łach, K. Korniejenko, J. Mikuła, Thermal insulation and thermally resistant materials made of geopolymer foams, Procedia Eng. 151 (2016) 410–416, https://doi.org/10.1016/j.proeng.2016.07.350.
[89] J. Henon, A. Alzina, J. Absi, D.S. Smith, S. Rossignol, Potassium geopolymer foams made with silica fume pore forming agent for thermal insulation, J. Porous Mater. 20 (2013) 37–46, https://doi.org/10.1007/s10934-012-9572-3.
[90] B. Nait-Ali, K. Haberko, H. Vesteghem, J. Absi, D.S. Smith, Preparation and thermal conductivity characterisation of highly porous ceramics: comparison between

experimental results, analytical calculations and numerical simulations, J. Eur. Ceram. Soc. 27 (2007) 1345–1350, https://doi.org/10.1016/j.jeurceramsoc.2006.04.025.

[91] Z.N.M. NGouloure, B. Nait-Ali, S. Zekeng, E. Kamseu, U.C. Melo, D. Smith, C. Leonelli, Recycled natural wastes in metakaolin based porous geopolymers for insulating applications, J. Build. Eng. 3 (2015) 58–69, https://doi.org/10.1016/j.jobe.2015.06.006.

[92] M. Romagnoli, P. Sassatelli, M. Lassinantti Gualtieri, G. Tari, Rheological characterization of fly ash-based suspensions, Construct. Build. Mater. 65 (2014) 526–534, https://doi.org/10.1016/j.conbuildmat.2014.04.130.

[93] E. Papa, V. Medri, D. Kpogbemabou, V. Morinière, J. Laumonier, A. Vaccari, S. Rossignol, Porosity and insulating properties of silica-fume based foams, Energy Build. 131 (2016) 223–232.

[94] E. Kamseu, Z.N.M. NGouloure, B.N. Ali, S. Zekeng, U.C. Melo, S. Rossignol, C. Leonelli, Cumulative pore volume, pore size distribution and phases percolation in porous inorganic polymer composites: relation microstructure and effective thermal conductivity, Energy Build. 88 (2015) 45–56, https://doi.org/10.1016/j.enbuild.2014.11.066.

[95] P. Posi, C. Teerachanwit, C. Tanutong, S. Limkamoltip, S. Lertnimoolchai, V. Sata, P. Chindaprasirt, Lightweight geopolymer concrete containing aggregate from recycle lightweight block, Mater. Des. 52 (2013) 580–586, https://doi.org/10.1016/j.matdes.2013.06.001.